

Zero-field splitting tensor of the triplet excited states of aromatic molecules: A valence full- π complete active space self-consistent field study

Katsuki Miyokawa^{*,†} and Yuki Kurashige^{*,†}

[†]*Department of Chemistry, Graduate School of Science, Kyoto University, Kitashirakawa
Oiwake-cho, Sakyo-ku Kyoto, 606-8502, Japan*

[‡]*CREST, JST, Honcho 4-1-8, Kawaguchi, Saitama 332-0012, Japan*

E-mail: miyokawa@theoc.kuchem.kyoto-u.ac.jp; kura@kuchem.kyoto-u.ac.jp

Abstract

A method to predict D tensor in the molecular frame with multiconfigurational wavefunctions in large active space was proposed, and spin properties of the lowest triplets of aromatic molecules were examined with full- π active space; such calculations were challenging because the size of active space grows exponentially with the number of π electrons. In the method, the exponential growth of the complexity is resolved by the density matrix renormalization group (DMRG) algorithm. From the D tensor, we can directly determine the direction of the magnetic axes and the ZFS parameters, D - and E -values, of the phenomenological spin Hamiltonian with their signs, which are not usually obtained in ESR experiments. The method using the DMRG-CASSCF wavefunction can give correct results even when the sign of D - and E -values are sensitive to the accuracy of the prediction of the D tensor and existing methods fail to predict the correct magnetic axes.

Introduction

Organic molecules in the lowest triplet state e.g., excited aromatic hydrocarbons, biradicals, and carbenes etc, are one of the most familiar paramagnetic species in the field of chemistry. The three spin sublevels are completely degenerate at the non-relativistic level, and the degeneracy is, albeit often very slightly, lifted by the relativistic effect, i.e., spin-spin coupling (SSC) and spin-orbit coupling (SOC). This is called zero-field splitting (ZFS) and is not only a factor in determining the spectrum of magnetic spectroscopy for paramagnetic species but also an important character for utilizing molecules in quantum information science.¹⁻³ In fact, photo-induced spin polarization to one of the three spin sublevels is efficiently realized for many planar aromatic hydrocarbons and for nitrogen-vacancy centers (NV-center) of synthetic diamond.⁴ This non-Boltzmann distributed polarization can be exploited in dynamic nuclear polarization (DNP)⁵⁻¹⁰ and MASER¹¹⁻¹³ operating under mild conditions. Also, in systems where a triplet chromophore encounters a radical species, electron spin polarization in the ground doublet state can be generated through the ZFS-driven mixing of the states.¹⁴⁻¹⁶ The energy gaps between electron spin sublevels, which are described by so-called ZFS parameters, affect the efficiency of polarization transfer in DNP experiment¹⁷ and the operating frequency of MASER. NV-center can maintain spin coherence at room temperature and is expected to be utilized as a qubit and quantum sensor.¹⁸ Considering the emergence of such application research, it has become important to accurately predict the ZFS D tensor that represents the splitting of electron spin sublevels by *ab initio* quantum chemical calculations. In particular, it is difficult to determine the correspondence between the principal axis of D tensor and the molecular orientation through experiments, whereas theoretical calculations can provide it. However, theoretical predictions of ZFS parameters are challenging due to the small magnitudes of spin interactions and the multiconfigurational character of the triplet state.

The dominant factor in determining the ZFS of organic, heavy element free, molecules is the electron SSC and the contribution of SOC is usually negligible. Early studies of electron

SSC in aromatic molecules were performed using semi-empirical approaches.^{19–23} However, the first calculation of ZFS parameters of triplet benzene using the *ab initio* configuration interaction (CI) method performed by Langhoff revealed that the comparative agreement with the experimental values in the semi-empirical calculation was coincidental.²⁴ It was also pointed out that the calculation of ZFS parameters was technically difficult because reliable description of spin density required a large number of configurations including in CI space, which was computationally too demanding that time. Later, larger-scale calculations became feasible with the advancement of computational technology, and since the 2000s, the calculations of electron SSC using modern quantum chemical methods, e.g., DFT, MCSCF and MRCI, has been reported.^{25–32} It was shown that calculations for aromatic hydrocarbons using ROHF and DFT yielded the *D*-values with large deviation from experimental measurements,^{33,34} which was attributed to the insufficient description of electron static correlation inherent in single reference wavefunction. In fact, Sinnecker and co-workers showed that whereas DFT calculations for oligoacenes resulted in values that were underestimated by approximately half compared to the experimental data, the CASSCF method gained some improvement.³⁵ In their calculations, the electron SSC was treated using a mean-field approximation, on the other hand, Vahtras and Loboda *et al.* derived the formalism using the two-particle density matrices, and demonstrated that by using large active space with RAS, *D*-values closer to the experimental ones were obtained for oligoacenes.^{29,30} Later, Ganyuishin developed the method for calculating larger molecules using the resolution of the identity approximation.³⁶

As mentioned above, the multi-configuration theories improve the accuracy of *D* tensor calculations of aromatic hydrocarbons, but may not reproduce experimental results when an insufficient number of π orbitals are included in the active space.^{37,38} The increase in active space requires immense computational costs, making it impractical to address large π -conjugated molecules. Density matrix renormalization group (DMRG) methods,³⁹ which utilizes tensor network technique to reduce the dimension of CI coefficients, can surpass

this limitation, and yield significant achievements in predicting spin-Hamiltonian parameters, e.g., electron g shift and hyperfine coupling constants, for molecules with large active space.^{40–43} Calculating SOC contribution to ZFS tensor with DMRG has been reported,^{44,45} but as far as we know, calculation of electron SSC using DMRG methods remains unreported. Here, in this work, we have implemented a method to calculate ZFS parameters from DMRG-CASSCF theory^{46–49} which can include all valence orbitals in active space, with the expectation of achieving high accuracy using DMRG methods. Calculated values were compared with experimental data to assess the accuracy of the method.

Theory

First, we will describe the definition of ZFS parameters of the phenomenological model Hamiltonian and its relationship with the energy gaps of triplet spin sublevels, and then, we will explain the equation used to calculate the matrix elements of D tensor contributed from electron SSC, and lastly, we will discuss our implementation in this work.

The phenomenological model Hamiltonian of ZFS is parameterized by the matrix \mathbf{D} and expressed as

$$\hat{H}_{\text{ZFS}} = \hat{\mathbf{S}}^\top \mathbf{D} \hat{\mathbf{S}}, \quad (1)$$

where \mathbf{S} is total spin operator. \mathbf{D} is a second-rank symmetric tensor and traceless due to the anisotropic nature of ZFS. When introducing a coordinate system that diagonalizes \mathbf{D} , this can be rewritten as

$$\hat{H}_{\text{ZFS}} = D_{XX} \hat{S}_X^2 + D_{YY} \hat{S}_Y^2 + D_{ZZ} \hat{S}_Z^2, \quad (2)$$

where D_{XX} , D_{YY} , and D_{ZZ} are the principal values of D tensor, and the capital letters XYZ denotes the principal axes. The three principal values are usually reduced to two ZFS

parameters D and E by using the traceless relation $D_{XX} + D_{YY} + D_{ZZ} = 0$. By setting

$$\begin{aligned} D &= D_{ZZ} - \frac{1}{2}(D_{XX} + D_{YY}), \\ E &= \frac{1}{2}(D_{XX} - D_{YY}), \end{aligned} \quad (3)$$

the ZFS Hamiltonian becomes

$$\hat{H}_{\text{ZFS}} = D \left(\hat{S}_Z^2 - \frac{1}{3} \hat{\mathbf{S}}^2 \right) + E \left(\hat{S}_X^2 - \hat{S}_Y^2 \right). \quad (4)$$

In the case of a triplet manifold, therefore, the eigenstates of the ZFS Hamiltonian are written as

$$|T_X\rangle = \frac{1}{\sqrt{2}} (|-1\rangle - |1\rangle), \quad |T_Y\rangle = \frac{i}{\sqrt{2}} (|-1\rangle + |1\rangle), \quad |T_Z\rangle = |0\rangle, \quad (5)$$

with the eigenvalues

$$\mathcal{E}(T_X) = \frac{D - E}{3}, \quad \mathcal{E}(T_Y) = \frac{D + E}{3}, \quad \mathcal{E}(T_Z) = -\frac{2D}{3}, \quad (6)$$

where $\mathcal{E}(T_\mu)$ ($\mu \in \{X, Y, Z\}$) represents the energy level of spin sublevel T_μ . Each state has zero eigenvalue of the spin projection \hat{S}_μ , which indicates that the spins are in precession in the plane perpendicular to the μ -axis. From Eq. (6), energy gaps between three spin sublevels are determined according to ZFS parameters. The sign of the ZFS parameters D and E depend on the labeling of the principal axes X, Y, Z for each energy level, and thus, it is common to impose constraints on the range of ZFS parameters

$$-\frac{1}{3} \leq \frac{E}{D} \leq 0. \quad (7)$$

It is equivalent to define the energy order of spin sublevels as $\mathcal{E}(T_Z) < \mathcal{E}(T_Y) < \mathcal{E}(T_X)$ for positive D -value and $\mathcal{E}(T_X) < \mathcal{E}(T_Y) < \mathcal{E}(T_Z)$ for negative D -value. It is sometimes convenient not to impose constraint (7). In this work, $X'Y'Z'$, and D', E' are used for the

ZFS principal axes that do not necessarily satisfy the constraint, in which the out-of-plane axis of the aromatic molecules is assigned to Z' (Table 3 and SI Figure 3-6).

Next, we will briefly explain the method for calculating the D tensor by *ab initio* calculations. The electron SSC term of the Breit-Pauli Hamiltonian is

$$\hat{H}_{\text{SSC}} = \frac{g_e^2 \mu_B^2 \alpha^2}{2} \sum_{i \neq j} \left[\frac{\hat{\mathbf{s}}(i) \cdot \hat{\mathbf{s}}(j)}{r_{ij}^3} - \frac{3(\hat{\mathbf{s}}(i) \cdot \mathbf{r}_{ij})(\hat{\mathbf{s}}(j) \cdot \mathbf{r}_{ij})}{r_{ij}^5} \right], \quad (8)$$

where g_e is electron g-factor, μ_B is Bohr magneton, α is fine structure constant, $\hat{\mathbf{s}}(i)$ is spin operator of electron i and \mathbf{r}_{ij} is a distance between electron i and j . In the following, atomic units will be used, where the Bohr magneton μ_B is 1/2. In the quasi-degenerate perturbation theory (QDPT), SSC contributes D tensor in the first-order and the element of the effective Hamiltonian is represented by $\langle \Psi_0^{SM} | \hat{H}_{\text{SSC}} | \Psi_0^{SM'} \rangle$, where subscript 0 indicates zeroth-order wavefunction. D tensor can be determined by assuming that the element of effective Hamiltonian is equal to that of the ZFS Hamiltonian $\langle SM | \hat{H}_{\text{ZFS}} | SM' \rangle$. Using the Wigner-Eckart theorem, the spin part of SSC Hamiltonian is transformed into the zeroth component of the second-rank spherical tensor, and the element of D tensor is expressed as

$$D_{kl}^{\text{SSC}} = \frac{g_e^2 \alpha^2}{4S(2S-1)} \langle \Psi_0^{SS} | \sum_{i \neq j} \frac{r_{ij}^2 \delta_{ij} - 3(\mathbf{r}_{ij})_k (\mathbf{r}_{ij})_l}{r_{ij}^5} \times [2\hat{s}_z(i)\hat{s}_z(j) - \hat{s}_x(i)\hat{s}_x(j) - \hat{s}_y(i)\hat{s}_y(j)] | \Psi_0^{SS} \rangle, \quad (9)$$

where subscript $k, l \in \{x, y, z\}$. In the second quantization formalism, Eq. (9) becomes

$$D_{kl}^{\text{SSC}} = \frac{g_e^2 \alpha^2}{4S(2S-1)} \sum_{pqrs} d_{pqrs}^{kl} q_{pqrs}, \quad (10)$$

where the indices $pqrs$ represent molecular orbitals, d_{pqrs}^{kl} is the two-electron, and q_{pqrs} is

constructed by two-body reduced density matrices

$$d_{pqrs}^{kl} = \iint \phi_p(\mathbf{r}_1) \phi_r(\mathbf{r}_2) \frac{r_{12}^2 \delta_{kl} - 3(\mathbf{r}_{12})_k (\mathbf{r}_{12})_l}{r_{12}^5} \phi_q(\mathbf{r}_1) \phi_s(\mathbf{r}_2) d\mathbf{r}_1 d\mathbf{r}_2, \quad (11)$$

$$q_{pqrs} = \frac{1}{4} \langle \Psi | E_{pq} \delta_{sr} - S_{ps}^z S_{rq}^z + \frac{1}{2} (S_{pq}^z S_{rs}^z - E_{pq} E_{rs}) | \Psi \rangle. \quad (12)$$

Once the D tensor is calculated and diagonalized, the ZFS parameters and principal axes are obtained by Eq. (3).

Lastly, we will discuss the implementation aspect of this work. The zeroth order wavefunctions used for D -tensor calculation were obtained from DMRG-CASSCF method, which was carried out using PySCF and BLOCK2 program packages.^{50–53} For the calculation of the integral d_{pqrs}^{kl} , RI approximation reported by Ganyushin *et al.* was used³⁶ to accelerate the integral transformation of large molecular systems. With the Coulomb metric, d_{pqrs}^{kl} can be decomposed to

$$d_{pqrs}^{kl} = \sum_{PQRS} g_P^{pq} (V^{-1})_{PQ} \langle Q | \hat{h}_{kl} | R \rangle (V^{-1})_{RS} g_S^{rs}, \quad (13)$$

where the indices $PQRS$ represent auxiliary basis, $g_P^{pq} = \langle pq | 1/r_{12} | P \rangle$, $V_{PQ} = \langle P | 1/r_{12} | Q \rangle$ and $\hat{h}_{kl} = \frac{r_{12}^2 \delta_{kl} - 3(\mathbf{r}_{12})_k (\mathbf{r}_{12})_l}{r_{12}^5}$. g_P^{pq} and V_{PQ} are the term that appeared in the standard calculation of the electron repulsion integral with the RI approximation, and are obtained directly from Libcint package.⁵⁰ The remaining two-center two-electron integral can be transformed as

$$\langle P | \hat{h}_{kl} | Q \rangle = \iint \phi_P(\mathbf{r}_1) \left[\frac{\partial^2}{\partial(\mathbf{r}_2)_k \partial(\mathbf{r}_1)_l} \frac{1}{r_{12}} \right] \phi_Q(\mathbf{r}_2) d\mathbf{r}_1 d\mathbf{r}_2. \quad (14)$$

As is well known, $1/r_{12}$ has a singularity at the origin and the second derivative yields the term proportional to the delta function. The form of this term resembles the Fermi-contact isotropic interaction and does not contribute to a D tensor for the traceless condition, and

thus it can be neglected. Here, using the translational invariance relation,

$$\left[\frac{\partial}{\partial(\mathbf{r}_2)_k} + \frac{\partial}{\partial(\mathbf{R}_P)_k} \right] \int \phi_P(\mathbf{r}_1) \frac{1}{r_{12}} d\mathbf{r}_1 = 0, \quad (15)$$

$$\left[\frac{\partial}{\partial(\mathbf{r}_1)_l} + \frac{\partial}{\partial(\mathbf{R}_Q)_l} \right] \int \frac{1}{r_{12}} \phi_Q(\mathbf{r}_2) d\mathbf{r}_2 = 0, \quad (16)$$

equation (14) becomes

$$\langle P | \hat{h}_{kl} | Q \rangle = \frac{\partial^2}{\partial(\mathbf{R}_P)_k \partial(\mathbf{R}_Q)_l} \langle P | \frac{1}{r_{12}} | Q \rangle. \quad (17)$$

The right-hand side is the derivative of the 2-center electron repulsion integral along the coordination of auxiliary basis ϕ_P and ϕ_Q , and was calculated from Libcint package. For the calculation of the quintet density q_{pqrs} , we used the spin-dependent two-electron reduced density matrices of the DMRG-CASSCF wavefunction.

Results and discussion

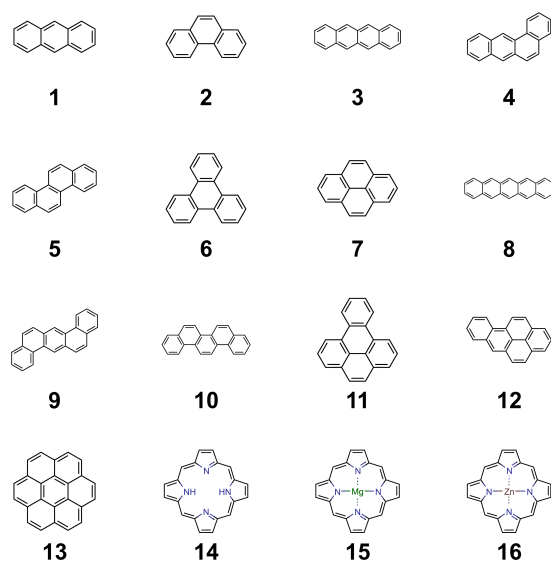


Figure 1: Structures of aromatic molecules which were selected for the calculation.

Sixteen aromatic molecules, of which experimental ZFS parameters in the triplet ex-

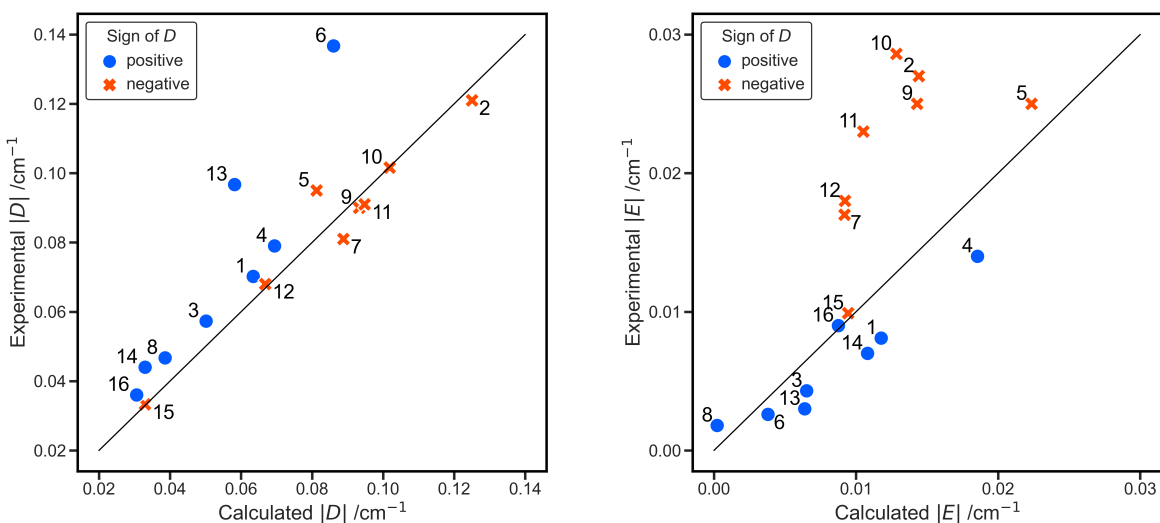


Figure 2: Scatter plot of calculated and experimental values of ZFS parameters for the selected organic molecules in triplet states.

cited state have been reported, were chosen as targets for benchmark (Figure 1). These include thirteen all-benzenoid polycyclic aromatic hydrocarbons (PAHs) and three porphyrins. Geometry optimizations of T_1 state were conducted at CASPT2(12,12)/cc-pVTZ(-f) level for oligoacenes and at the time-dependent density functional theory (TD-DFT) with LC-BLYP/def2-TZVP for other molecules. The TD-DFT calculations were carried out using ORCA5.0.3 program package and the range-separation parameter μ of the functional was set to 0.15. For each molecule, natural orbitals obtained from the diagonalization of MP2 density matrix or atomic valence active space (AVAS) module in PySCF, which automatically construct active space, were used for extracting valence π orbitals. As usual in DMRG method, all valence π orbitals were localized and manually ordered (SI Figure 1). Then, DMRG-CASSCF calculations with cc-pVDZ basis set were carried out with bond dimension $M = 1024$ and cc-pVDZ-jk-fit auxiliary basis sets.⁵⁴ Subsequent calculations of ZFS parameters implemented in this work were carried out using cc-pVQZ-jk-fit auxiliary basis, which should be sufficient to disregard the errors from the RI approximation. As the jk-fit basis for Mg and Zn atoms cc-pVQZ-RIFIT auxiliary basis sets⁵⁴ were used for both. The results of the calculated ZFS parameters are summarized in Table 1 and Figure 2. In the

table, $\eta = |E/D|$ and the sign of D -values from experiment are listed to be all positive. In the figure, the color of the dots represent the sign of D -value theoretically predicted (blue indicates positive and orange indicates negative).

Table 1: The ZFS paramters of T_1 state of the π conjugated molecules by the DMRG-CASSCF theory with full- π active space and bond dimension $M=1024$. In the calculation of RMSD and MAPE, it was assumed that the sign of the experimental D -values are the same as the predicted ones.

No.	Molecule	Theoretical			Experimental			Ref.
		D /cm ⁻¹	E /cm ⁻¹	η	$ D $ /cm ⁻¹	$ E $ /cm ⁻¹	η	
1	Anthracene	0.0634	-0.0118	0.19	0.0702	0.0081	0.12	[55]
2	Phenanthrene	-0.1250	0.0144	0.12	0.121	0.027	0.22	[22]
3	Tetracene	0.0502	-0.0065	0.13	0.0573	0.0043	0.08	[56]
4	1,2-BA	0.0694	-0.0186	0.27	0.079	0.014	0.18	[22]
5	Chrysene	-0.0813	0.0224	0.28	0.095	0.025	0.26	[22]
6	Triphenylene	0.0861	-0.0038	0.04	0.1367	0.0026	0.02	[57]
7	Pyrene	-0.0888	0.0092	0.10	0.081	0.017	0.21	[22]
8	Pentacene	0.0386	-0.0002	0.01	0.0467	0.0018	0.04	[58]
9	1,2,5,6-DBA	-0.0933	0.0143	0.15	0.090	0.025	0.28	[22]
10	Picene	-0.1019	0.0128	0.13	0.1016	0.0286	0.28	[59]
11	1,2-BP	-0.0948	0.0105	0.11	0.091	0.023	0.26	[60]
12	3,4-BP	-0.0668	0.0092	0.14	0.068	0.018	0.26	[61]
13	Coronene	0.0582	-0.0064	0.11	0.0967	0.0030	0.03	[62]
14	Porphyrin	0.0330	-0.0108	0.33	0.044	0.007	0.16	[63]
15	Mg porphyrin	-0.0330	0.0094	0.29	0.0333	0.0099	0.30	[64]
16	Zn porphyrin	0.0306	-0.0088	0.29	0.036	0.009	0.25	[65]
	RMSD	0.0172	0.0075	0.10				
	MAPE	12.9%	46.4%	68.0%				

To evaluate the deviation from the experimental results, root mean square deviation (RMSD) and mean absolute percentage error (MAPE) were calculated under the assumption that the signs of the experimental are identical to the calculated values. The RMSD

(MAPE) are 0.0172 cm⁻¹(12.9%), 0.0075 cm⁻¹(46.4%) for D -value and E -value , respectively. Because the absolute value of E -value is smaller than D -value, RMSD of E -value is smaller than that of D -value and MAPE of E -value was larger than that of D -value. For comparison with existing methods, the calculations of ZFS parameters were performed at LC-BLYP($\mu=0.15$)/cc-pVDZ level and CASSCF(12,12)/cc-pVDZ level. With the former approach, the deviation was 0.0422 cm⁻¹(44.0%), 0.0119 cm⁻¹(76.5%), and with the latter approach, the deviation was 0.0284 cm⁻¹(28.1%), 0.0091 cm⁻¹(51.5%) for D -value and E -value respectively (SI Table 1). Therefore, compared to DFT and CASSCF with small active spaces, DMRG-CASSCF with full- π active space predicted the ZFS parameters more accurately. The improvement in accuracy was particularly significant for the D -value while the improvement in the E -value was relatively smaller, which indicated the difficulty of predicting E -values and suggested that further increase in computational level may be necessary for accurate predictions.

Next, we will discuss the trends of the error. For all the aromatic molecules calculated, the out-of-plane direction is one of the principal axes, and the energetically lowest sublevel in all cases, i.e. it is assigned to Z -axis for the molecules with $D > 0$ and X -axis for those with $D < 0$. To analyze the trend of the error based on the molecular structure, we therefore labeled the out-of-plane axis as Z' and in-plane axes as X' and Y' , and defined the ZFS parameters as

$$\begin{aligned} D' &= \frac{\mathcal{E}(T_{Y'}) + \mathcal{E}(T_{X'})}{2} - \mathcal{E}(T_{Z'}), \\ E' &= \frac{\mathcal{E}(T_{Y'}) - \mathcal{E}(T_{X'})}{2}, \end{aligned} \quad (18)$$

instead of imposing the constraint Eq (6). Theoretical predictions of $|D'|$ tended to underestimate the experimental values, while those of $|E'|$ tended to overestimate them with some exceptions (SI Figure 3 and 4). E' of chrysene (5) deviates from the trend, but the absolute value of the deviation is small. Relatively large deviation in D' -values were found in triphenylene (6) and coronene (13). Triphenylene and coronene have the symmetry axes with

more than three-fold rotation and have orbitally degenerated low-lying triplet states. The coupling of electronic states between quasi-degenerate states, e.g, SOC and spin-vibronic coupling, could affect D -tensor.³⁴ This type of error is also possible in some porphyrins, where T_1 and T_2 states are nearly degenerated. Also, according to the report by Gastel, it was pointed out that ZFS parameters of aromatic molecules are influenced by $\sigma - \pi$ polarization.⁶⁶ This discrepancy could potentially be decreased by incorporating dynamical electron correlation, which is one of the future challenges. Several trends were observed in the relationship between molecular structures and ZFS parameters. Conventionally, it has been known that by assuming the classical point dipole approximation and the appropriate axis, ZFS parameters arising from SSC can be expressed as follows.

$$\begin{aligned} D &= \frac{3\mu_0}{16\pi\hbar} (g_e\mu_B)^2 \left\langle \frac{r^2 - 3z^2}{r^5} \right\rangle, \\ E &= \frac{3\mu_0}{16\pi\hbar} (g_e\mu_B)^2 \left\langle \frac{y^2 - x^2}{r^5} \right\rangle. \end{aligned} \quad (19)$$

From Eq. (19), it is commonly said that D - and E -value depend on the average distance between spins and the rhombicity of spin density, respectively. In the series of the oligoacenes, this is true for the D -values, but not for the E -values because both D and E become small as the number of rings increases. In particular, the E -value of a pentacene is quite small comparable to that of triphenylene and coronene which have nearly zero E -values due to their three-fold or higher rotational symmetry. The decrease in D -value of oligoacenes can be explained by the delocalization of the spin density with the extension of π plane, but the decrease in E -value cannot be explained from the perspective that the E -value is an indicator of axial symmetry. Bräuchle *et al.* explained that as the spin distribution spreads in the x -axis direction, which is the long axis direction of the oligoacene, E -value asymptotically approaches $(y^2 - x^2)/r^5 \rightarrow -1/x^3$, and thus E -value decreases by the elongation of oligoacenes.⁶⁰ In other words, the expansion of spin density leads to the larger denominator, causing the decrease in the E -value. Bräuchle *et al.* also noted that the magnitude of the D -value of a PAH is related to the number of Clar's sextet.⁶⁷ The Clar's rule is an empirical

rule that has been known for decades, stating that among the resonance structures of PAHs, the structure with the highest number of disjoint benzene-like π sextets is the most important to describe their properties.⁶⁸ Although whether the Clar’s rule can simply be applied to the properties in excited states is a matter of debate, it was observed that the molecules with a larger number of the Clar’s sextets exhibited a larger D -value than other molecules with the same number of π orbitals. (SI Figure 8). Oligoacenes have only one Clar’s sextet, which corresponds to the fact that the D -value is smaller compared to other isomers with the same number of carbon atoms. Porphyrin shows a smaller D -value than the other all-benzenoid PAHs, and the η is close to $1/3$. The Fermi level of porphyrins has traditionally been described by Gouterman’s four-orbital model, where HOMO and HOMO-1, as well as LUMO and LUMO+1, are nearly degenerate. In the triplet state, the Jahn-Teller effect lifts the energy degeneracy, resulting in in-plane structural distortion. This distortion leads to an increase in E -value which characterizes the axituality.⁶⁹ It should be noted that the ZFS parameters are not necessarily accounted for by the distribution of the spin density, which is a one-body property, because the SSC is a two-body interaction.

Table 2: Convergence behavior of the DMRG-CASSCF energy and ZFS parameters for the anthracene and the phenanthrene to the large M limit.

		256	512	1024	2048	FCI	Exp.
Anthracene	$\mathcal{E}(T_1)$ /cm ⁻¹	1.4661	0.0567	0.0009	<10 ⁻⁴	0	
	D /cm ⁻¹	0.0586	0.0618	0.0634	0.0642	0.0643	0.0702
	E /cm ⁻¹	-0.0088	-0.0110	-0.0118	-0.0121	-0.0122	-0.0081
Phenanthrene	$\mathcal{E}(T_1)$ /cm ⁻¹	23.7229	1.5722	0.0393	0.0006	0	
	D /cm ⁻¹	-0.1245	-0.1255	-0.1250	-0.1252	-0.1253	-0.121
	E /cm ⁻¹	0.0108	0.0134	0.0144	0.0150	0.0151	0.027

Next, we will discuss the convergence behavior of ZFS parameters against the bond dimension M . Table 2 summarizes the changes in ZFS parameters for anthracene and phenanthrene when the various bond dimensions from 256 to 2048. The energy values are expressed relative to the values of CASSCF(14,14). It was found that with increasing the bond di-

mension, the convergence of the ZFS parameters is slower compared to the convergence of the energy. On the other hand, the D -value of phenanthrene is coincidentally closer to the values of FCI with a small bond dimension, and this indicates that the error cancellation may occur in the calculation of the ZFS parameters using the DMRG-CASSCF method. There is a possibility to improve the convergence behavior along the bond dimension if the D tensor is evaluated using non-perturbative manner, which can be achieved by diagonalizing the Hamiltonian including both non-relativistic term and SSC term in the CASCI space, like spin-orbit configuration interaction (SOC) approach.⁷⁰

Table 3: ZFS parameters for the pentacene at the different calculation levels.

	D' / cm^{-1}	E' / cm^{-1}	η	$\mathcal{E}(\text{T}_1) / \text{Eh}$
DFT	0.0286	0.0025	0.09	
CASSCF(4,4)	0.0286	0.0059	0.21	-841.317403
CASSCF(8,8)	0.0307	0.0080	0.26	-841.383524
CASSCF(12,12)	0.0354	0.0050	0.14	-841.416827
CASSCF(14,14)	0.0371	-0.0021	0.06	-841.442815
CASSCF(16,16)	0.0402	-0.0029	0.07	-841.476852
DMRG-CASSCF(18,18) ^a	0.0374	0.0037	0.10	-841.505719
DMRG-CASSCF(22,22) ^b	0.0386	-0.0002	0.01	-841.577315
DMRG-CASSCF(22,22) ^c	0.0398	-0.0009	0.02	-841.577315
Exp. ^d	0.0467	-0.0018	0.04	

^a $M = 2048$; ^b $M = 1024$; ^c $M = 1536$; ^d Ref[58];

The values of ZFS parameters obtained for pentacene with different active space are shown in Table 3. D' and E' are defined by Eq (18) where X' , Y' and Z' correspond to the long axis, short axis, and out-of-plane axis of the pentacene, respectively. As the size of the active space increases, the predicted D' -values also increase to be close to the experimental value. It can be seen that the contribution of the π orbitals away from the Fermi level is also important for describing the two-electron SSC. Also, D' -value of DMRG-CASSCF(22,22) does not obey the tendency, which may be caused from the lack of bond

dimension. With increasing the active space further, the sign of the predicted E' -values changed from plus to minus, which corresponds to the energy reversal of two spin sublevels at in-plane from $T_{X'} < T_{Y'}$ to $T_{Y'} < T_{X'}$. The experiments showed that the highest energy of the sublevels is in the long-axis direction, so the result of full- π active space correctly predicts the experimental energy ordering. The same behavior is also observed in the DMRG-CASSCF(22,22) with respect to the increase in the bond dimension. Thus, small active space or insufficient bond dimension can provide qualitatively incorrect energy order of the spin sublevels when E is very small. Comparing the results of DFT and DMRG-CASSCF with the full- π active space, DFT failed to predict the sign of E -value for the molecules with the small E , e.g. tetracene, triphenylene, pentacene, and coronene (Figure 5S and 6S), and the sign of D -value for the molecules with $\eta \approx 1/3$, e.g. free-base, Mg, and Zn porphyrins and chrysene. In such conditions, the sign of ZFS parameters are quite sensitive to the accuracy of the predicted D -tensor.

Conclusion

In this work, the method for the accurate prediction of the ZFS parameters using the DMRG-CASSCF theory was proposed and examined for the aromatic molecules in the lowest triplet states with the valence full- π active space. The accuracy of the prediction of D tensor increases as increasing the size of the active space. The DMRG-CASSCF calculations with the large active space yielded closer values to the experimental results than the DFT or CASSCF calculations with small active space. In fact, in particular for the systems where E is small or η close to $1/3$, the signs of the ZFS parameters D and E were sensitive to the accuracy of the prediction of the D tensor, and the DFT and CASSCF with the small active space failed to predict the correct sign for the ZFS parameters, e.g. the E values of the oligoacenes and the D values of the porphyrins and chrysene. For those systems, the DMRG-CASSCF method is required to achieve reliable prediction for the ZFS parameters.

In the DMRG-CASSCF calculations, it was observed that the larger bond dimension was required to obtain sufficiently converged results for the ZFS parameters as compared to the energy expectation value of the non-relativistic Hamiltonian. That could be because the DMRG-CASSCF wavefunctions are not optimized to describe the SSC, which is absent in the non-relativistic Hamiltonian, and the convergence can be improved if the SSC Hamiltonian is incorporated into the DMRG algorithm.

As a future work, the developed method can be applied to metal complex systems, where DMRG-CASSCF exhibits its power due to the ability to treat large active space. It is known that the contribution of SSC is small but not negligible compared to SOC in metal complex systems.⁷¹ We believe that the ability to accurately predict ZFS parameters and principal axes with the method developed in this work will aid in the practical application of quantum technology.

Acknowledgement

This work was partly supported by the JST-FOREST Program (JPMJFR221R), JST-CREST Program (JPMJCR23I6), and MEXT Q-LEAP Program (JPMXS0120319794).

Supporting Information Available

References

- (1) Wasielewski, M. R. et al. Exploiting chemistry and molecular systems for quantum information science. *Nat. Rev. Chem.* **2020**, *4*, 490–504.
- (2) Wang, Z.; Zhang, X.; Zhao, J. Electron Spin Dynamics of the Intersystem Crossing of Triplet Photosensitizers That Show Strong Absorption of Visible Light and Long-Lived Triplet States. *J. Phys. Chem. C* **2021**, *125*, 19097–19109.

- (3) Scholes, G. D. A molecular perspective on quantum information. *Proc. Math. Phys. Eng. Sci.* **2023**, *479*, 20230599.
- (4) Eills, J.; Budker, D.; Cavagnero, S.; Chekmenev, E. Y.; Elliott, S. J.; Jannin, S.; Lesage, A.; Matysik, J.; Meersmann, T.; Prisner, T.; Reimer, J. A.; Yang, H.; Kopyug, I. V. Spin Hyperpolarization in Modern Magnetic Resonance. *Chem. Rev.* **2023**, *123*, 1417–1551.
- (5) Henstra, A.; Dirksen, P.; Wenckebach, W. T. Enhanced dynamic nuclear polarization by the integrated solid effect. *Phys. Lett. A* **1988**, *134*, 134–136.
- (6) Henstra, A.; Lin, T.-S.; Schmidt, J.; Wenckebach, W. T. High dynamic nuclear polarization at room temperature. *Chem. Phys. Lett.* **1990**, *165*, 6–10.
- (7) Iinuma, M.; Takahashi, Y.; Shaké, I.; Oda, M.; Masaike, A.; Yabuzaki, T.; Shimizu, H. M. Proton polarization with p-terphenyl crystal by integrated solid effect on photoexcited triplet state. *J. Magn. Reson.* **2005**, *175*, 235–241.
- (8) Takeda, K. *Triplet State Dynamic Nuclear Polarization*; VDM Verlag Dr. Mueller, 2009.
- (9) Tateishi, K.; Negoro, M.; Kagawa, A.; Kitagawa, M. Dynamic Nuclear Polarization with Photoexcited Triplet Electrons in a Glassy Matrix. *Angew. Chem. Int. Ed.* **2013**, *52*, 13307–13310.
- (10) Nishimura, K.; Kouno, H.; Kawashima, Y.; Orihashi, K.; Fujiwara, S.; Tateishi, K.; Uesaka, T.; Kimizuka, N.; Yanai, N. Materials chemistry of triplet dynamic nuclear polarization. *Chem. Commun.* **2020**, *56*, 7217–7232.
- (11) Oxborrow, M.; Breeze, J. D.; Alford, N. M. Room-temperature solid-state maser. *Nature* **2012**, *488*, 353–356.
- (12) Breeze, J.; Tan, K.-J.; Richards, B.; Sathian, J.; Oxborrow, M.; Alford, N. M. Enhanced magnetic Purcell effect in room-temperature masers. *Nat. Commun.* **2015**, *6*, 6215.

- (13) Bogatko, S.; Haynes, P. D.; Sathian, J.; Wade, J.; Kim, J.-S.; Tan, K.-J.; Breeze, J.; Salvadori, E.; Horsfield, A.; Oxborrow, M. Molecular Design of a Room-Temperature Maser. *2016*, *120*, 8251–8260.
- (14) Yamauchi, A.; Fujiwara, S.; Nishimura, K.; Sasaki, Y.; Tateishi, K.; Uesaka, T.; Kimizuka, N.; Yanai, N. Design Guidelines to Elongate Spin–Lattice Relaxation Times of Porphyrins with Large Triplet Electron Polarization. *J. Phys. Chem. A* **2021**, *125*, 4334–4340.
- (15) Hamachi, T.; Nishimura, K.; Kouno, H.; Kawashima, Y.; Tateishi, K.; Uesaka, T.; Kimizuka, N.; Yanai, N. Porphyrins as Versatile, Aggregation-Tolerant, and Biocompatible Polarizing Agents for Triplet Dynamic Nuclear Polarization of Biomolecules. *J. Phys. Chem. Lett.* **2021**, *12*, 2645–2650.
- (16) Nishimura, K.; Yabuki, R.; Hamachi, T.; Kimizuka, N.; Tateishi, K.; Uesaka, T.; Yanai, N. Dynamic Electron Polarization Lasting More Than 10 Ms by Hybridizing Porphyrin and TEMPO with Flexible Linkers. *J. Phys. Chem. B* **2023**, *127*, 1219–1228.
- (17) Sakamoto, K.; Hamachi, T.; Miyokawa, K.; Tateishi, K.; Uesaka, T.; Kurashige, Y.; Yanai, N. Polarizing agents beyond pentacene for efficient triplet dynamic nuclear polarization in glass matrices. *PNAS* **2023**, *120*, e2307926120.
- (18) Budker, D.; Romalis, M. Optical magnetometry. *Nat. Phys.* **2007**, *3*, 227–234.
- (19) Hameka, H. F. Theory of the Electron Spin Resonance of Benzene in the Triplet State. *J. Chem. Phys.* **1959**, *31*, 315–321.
- (20) Godfrey, M.; Kern, C. W.; Karplus, M. Studies of Zero-Field Splittings in Aromatic Molecules. *J. Chem. Phys.* **1966**, *44*, 4459–4469.

- (21) Thomson, C. Zero-field splittings in aromatic triplet states: I. Naphthalene, pyrene and 1,12-benzperylene. *Mol. Phys.* **1966**, *10*, 309.
- (22) Brinen, J. S.; Orloff, M. K. Zero-Field Splitting in Phosphorescent Triplet States of Aromatic Hydrocarbons. *J. Chem. Phys.* **1966**, *45*, 4747–4750.
- (23) van der Waals, J. H.; Ter Maten, G. Zero-field splitting of the lowest triplet state of some aromatic hydrocarbons: Calculation and comparison with experiment. *Mol. Phys.* **1964**, *8*, 301–318.
- (24) Langhoff, S. R. Zero Field Splitting of the Triplet State of Porphyrins. II. *J. Chem. Phys.* **1975**, *62*, 169.
- (25) Petrenko, T. T.; Petrenko, T. L.; Bratus', V. Y. The carbon $\langle 100 \rangle$ split interstitial in SiC. *J. Phys. Condens. Matter* **2002**, *14*, 12433.
- (26) Shoji, M.; Koizumi, K.; Hamamoto, T.; Taniguchi, T.; Takeda, R.; Kitagawa, Y.; Kawakami, T.; Okumura, M.; Yamanaka, S.; Yamaguchi, K. A theoretical study of zero-field splitting of organic biradicals. *Polyhedron* **2005**, *24*, 2708–2715.
- (27) Sugisaki, K.; Toyota, K.; Sato, K.; Shiomi, D.; Kitagawa, M.; Takui, T. Ab initio and DFT studies of the spin–orbit and spin–spin contributions to the zero-field splitting tensors of triplet nitrenes with aryl scaffolds. *Phys. Chem. Chem. Phys.* **2011**, *13*, 6970–6980.
- (28) Reynolds, R. D.; Shiozaki, T. Zero-Field Splitting Parameters from Four-Component Relativistic Methods. *J. Chem. Theory Comput.* **2019**, *15*, 1560–1571.
- (29) Vahtras, O.; Loboda, O.; Minaev, B.; Ågren, H.; Ruud, K. Ab Initio Calculations of Zero-Field Splitting Parameters. *Chem. Phys.* **2002**, *279*, 133–142.

- (30) Loboda, O.; Minaev, B.; Vahtras, O.; Schimmelpfennig, B.; Ågren, H.; Ruud, K.; Jonsson, D. Ab Initio Calculations of Zero-Field Splitting Parameters in Linear Polyacenes. *Chem. Phys.* **2003**, *286*, 127–137.
- (31) Gilka, N.; Taylor, P. R.; Marian, C. M. Electron spin-spin coupling from multireference configuration interaction wave functions. *J. Chem. Phys.* **2008**, *129*, 044102.
- (32) Lang, L.; Neese, F. Spin-dependent properties in the framework of the dynamic correlation dressed complete active space method. *J. Chem. Phys.* **2019**, *150*, 104104.
- (33) Loboda, O.; Tunell, I.; Minaev, B.; Ågren, H. Theoretical study of triplet state properties of free-base porphyrin. *Chem. Phys.* **2005**, *312*, 299–309.
- (34) Perumal, S.; Minaev, B.; Ågren, H. Spin-spin and spin-orbit interactions in nanographene fragments: A quantum chemistry approach. *J. Chem. Phys.* **2012**, *136*, 104702.
- (35) Sinnecker, S.; Neese, F. Spin-Spin Contributions to the Zero-Field Splitting Tensor in Organic Triplets, Carbenes and Biradicals A Density Functional and Ab Initio Study. *J. Phys. Chem. A* **2006**, *110*, 12267–12275.
- (36) Ganyushin, D.; Neese, F. First-Principles Calculations of Zero-Field Splitting Parameters. *J. Chem. Phys.* **2006**, *125*, 024103.
- (37) Perumal, S. S.; Minaev, B.; Vahtras, O.; Ågren, H. Spin-spin coupling in 3b2 state of oxyallyl – A comparative study with trimethylenemethane. *Comput. Theor. Chem.* **2011**, *963*, 51–54.
- (38) Redman, A. J.; Moise, G.; Richert, S.; Viere, E. J.; Myers, W. K.; Therien, M. J.; Timmel, C. R. EPR of Photoexcited Triplet-State Acceptor Porphyrins. *J. Phys. Chem. C* **2021**, *125*, 11782–11790.

- (39) White, S. R. Density matrix formulation for quantum renormalization groups. *Phys. Rev. Lett.* **1992**, *69*, 2863–2866.
- (40) Roemelt, M. Spin orbit coupling for molecular *ab initio* density matrix renormalization group calculations: Application to g-tensors. *J. Chem. Phys.* **2015**, *143*, 044112.
- (41) Sayfutyarova, E. R.; Chan, G. K.-L. Electron paramagnetic resonance g-tensors from state interaction spin-orbit coupling density matrix renormalization group. *J. Chem. Phys.* **2018**, *148*, 184103.
- (42) Lan, T. N.; Kurashige, Y.; Yanai, T. Toward Reliable Prediction of Hyperfine Coupling Constants Using *Ab Initio* Density Matrix Renormalization Group Method: Diatomic $^2\Sigma$ and Vinyl Radicals as Test Cases. *J. Chem. Theory Comput.* **2014**, *10*, 1953–1967.
- (43) Nguyen Lan, T.; Kurashige, Y.; Yanai, T. Scalar Relativistic Calculations of Hyperfine Coupling Constants Using Ab Initio Density Matrix Renormalization Group Method in Combination with Third-Order Douglas–Kroll–Hess Transformation: Case Studies on 4d Transition Metals. *J. Chem. Theory Comput.* **2015**, *11*, 73–81.
- (44) Sayfutyarova, E. R.; Chan, G. K.-L. A state interaction spin-orbit coupling density matrix renormalization group method. *J. Chem. Phys.* **2016**, *144*, 234301.
- (45) Zhai, H.; Chan, G. K.-L. A comparison between the one- and two-step spin-orbit coupling approaches based on the *ab initio* density matrix renormalization group. *J. Chem. Phys.* **2022**, *157*, 164108.
- (46) Ghosh, D.; Hachmann, J.; Yanai, T.; Chan, G. K.-L. Orbital optimization in the density matrix renormalization group, with applications to polyenes and β -carotene. **2008**, *128*, 144117.
- (47) Zgid, D.; Nooijen, M. The density matrix renormalization group self-consistent field

- method: Orbital optimization with the density matrix renormalization group method in the active space. *J. Chem. Phys.* **2008**, *128*, 144116.
- (48) Yanai, T.; Kurashige, Y.; Ghosh, D.; Chan, G. K.-L. Accelerating convergence in iterative solution for large-scale complete active space self-consistent-field calculations. *Int. J. Quantum Chem.* **2009**, *109*, 2178–2190.
- (49) Marti, K. H.; Ondík, I. M.; Moritz, G.; Reiher, M. Density Matrix Renormalization Group Calculations on Relative Energies of Transition Metal Complexes and Clusters. *J. Chem. Phys.* **2008**, *128*, 014104.
- (50) Sun, Q. Libcint: An efficient general integral library for Gaussian basis functions. *J. Comput. Chem.* **2015**, *36*, 1664–1671.
- (51) Sun, Q.; Berkelbach, T. C.; Blunt, N. S.; Booth, G. H.; Guo, S.; Li, Z.; Liu, J.; McClain, J. D.; Sayfutyarova, E. R.; Sharma, S.; Wouters, S.; Chan, G. K.-L. PySCF: the Python-based simulations of chemistry framework. *WIREs Comput. Mol. Sci.* **2018**, *8*, e1340.
- (52) Sun, Q. et al. Recent developments in the PySCF program package. **2020**, *153*, 024109.
- (53) Zhai, H.; Chan, G. K.-L. Low communication high performance ab initio density matrix renormalization group algorithms. **2021**, *154*, 224116.
- (54) Pritchard, B. P.; Altarawy, D.; Didier, B.; Gibson, T. D.; Windus, T. L. New Basis Set Exchange: An Open, Up-to-Date Resource for the Molecular Sciences Community. *J. Chem. Inf. Model.* **2019**, *59*, 4814–4820.
- (55) S.P. McGlynn, T. A.; Kkinoshita, M. *Molecular spectroscopy of the triplet state*; Prentice-Hall, 1969.
- (56) Clarke, R. H.; Frank, H. A. Triplet state radiationless transitions in polycyclic hydrocarbons. *J. Chem. Phys.* **2008**, *65*, 39–47.

- (57) Nishi, N.; Matsui, K.; Kinoshita, M.; Higuchi, J. Study on the triplet state of triphenylene by microwave induced delayed phosphorescence and T←S excitation spectroscopy. *Mol. Phys* **1979**, *38*, 1–24.
- (58) Sloop, D. J.; Yu, H.; Lin, T.; Weissman, S. I. Electron Spin Echoes of a Photoexcited Triplet: Pentacene in *p*-terphenyl Crystals. *J. Chem. Phys.* **1981**, *75*, 3746–3757.
- (59) Kim, S. The triplet state of picene in *p*-terphenyl crystals by EPR. *Chem. Phys. Lett.* **1979**, *61*.
- (60) Bräuchle, C.; Kabza, H.; Voitländer, J. A concept to explain the variation of the triplet zero-field splitting parameters with the structure of aromatic hydrocarbons in terms of local benzenoid characteristics. *Chem. Phys.* **1980**, *48*, 369–385.
- (61) Clarke, R. H.; Hayes, J. M. Triplet state dynamics in polycyclic aromatic molecules. *Chem. Phys. Lett.* **1974**, *27*, 556–561.
- (62) Ohno, K.; Nishi, N.; Kinoshita, M.; Inokuchi, H. Study of radiative properties of the phosphorescent coronene in *n*-octane by microwave induced delayed phosphorescence. *Chem. Phys. Lett.* **1975**, *33*, 293–297.
- (63) Langhoff, S. R. Zero field splitting of the triplet state of porphyrins. II. *J. Chem. Phys.* **1975**, *62*, 169.
- (64) van der Waals, J.; van Dorp, W.; Schaafsma, T. In *The Porphyrins, Vol. IV*; Dolphin, D., Ed.; Academic Press, 1979; pp 257–312.
- (65) Chan, I.; van Dorp, W.; Schaafsma, T.; van der Waals, J. The lowest triplet state of Zn porphin. *Mol. Phys.* **1971**, *22*, 753–760.
- (66) van Gastel, M. The effect of spin polarization on zero field splitting parameters in paramagnetic π -electron molecules. *J. Chem. Phys.* **2009**, *131*, 124111.

- (67) Bräuchle, C.; Kabza, H.; Voitländer, J. A Concept to Relate the ZFS Parameter D of Aromatic Hydrocarbons to Molecular and Electronic Structure. *Z. Naturforsch. A* **1979**, *34*, 265–268.
- (68) Solà, M. Forty years of Clar's aromatic π -sextet rule. *Front. Chem.* **2013**, *1*.
- (69) Nguyen, K. A.; Pachter, R. Jahn–Teller Triplet Excited State Structures and Spectra of Zinc Complexes of Porphyrin and Phthalocyanine: A Density Functional Theory Study. *J. Chem. Phys.* **2003**, *118*, 5802–5810.
- (70) Sjøvoll, M.; Gropen, O.; Olsen, J. A determinantal approach to spin-orbit configuration interaction. *Theor. Chem. Acc.* **1997**, *97*, 301–312.
- (71) Neese, F. Importance of Direct Spin-Spin Coupling and Spin-Flip Excitations for the Zero-Field Splittings of Transition Metal Complexes: A Case Study. *J. Am. Chem. Soc.* **2006**, *128*, 10213–10222.